Journal of Materials Chemistry B

Accepted Manuscript

ROYAL SOCIETY OF CHEMISTRY

www.rsc.org/materialsB

Development of molecularly imprinted polymer nanoarrays of N-acryloyl-2-mercaptobenzamide on silver electrode for ultratrace sensing of uracil and 5-fluorouracil

Bhim Bali Prasad*[a] and Anil Kumar[a]

[a]*Analytical Division, Department of Chemistry, Faculty of Science, Banaras Hindu University, Varanasi-221005, India*

Abstract

The present work describes a new, simple and easy method for the generation of novel molecularly imprinted polymer-based nanoarrays with uracil and 5-fluorouracil as template(s) on the surface of silver electrode. The procedure involved an electrochemical etching of silver-wire to develop nanopores on its tip. In these nanopores, a prepolymer mixture with template(s) was filled-in via spin coating and subjected to the free radical thermal polymerization. The bulk polymer and polymer film characteristics were investigated using Fourier transform infrared spectroscopy, X-ray photoelectron spectroscopy, scanning electron microscopy, and atomic force microscopy. The prepolymerization complex stoichiometry involved one template molecule and two molecules of the N-acryloyl-2-mercaptobenzamide functional monomer. Molecular structure of this complex was thermodynamically optimized via density functional theory at MP2/6-31+G (d, p) level. The nanoarrays, vertically tethered imprinted polymer brush with embedded carbon nanotubes, helped enhancing surface area of the electrode. This drastically facilitated unhindered vertical diffusion with selective binding of uracil and 5-fluorouracil and their sensitive analysis using differential pulse anodic stripping voltammetry, with detection limits as low as 0.50 and 0.33 ng mL^{-1} (S/N=3), respectively. The proposed nanoscale electro-chemical sensor was also validated with the complex matrices of blood plasma and pharmaceutics which assured reliable results, without any matrix effect, cross-reactivity, and false-positives. The large therapeutic range of test analyte (uracil 1.49-278.76 ng mL^{-1}, 5-fluorouracil 1.33-401.15 ng mL^{-1}), demonstrating a perfect linearity (R^2= 0.98) with the improved voltammetric response, merits special significance for the primitive diagnosis of several chronic diseases, in clinical settings, without any sample pretreatment.

*Corresponding author. E-mail address: prof.bbpd@yahoo.com Phone +91 9451954449; Fax: +91 542 22368127

1. Introduction

Molecular imprinting polymerization technique has been in the focus of intense research in recent years; this has been developed for the preparation of selective separation materials and as sensing layers in sensor devices. Our interest in sensitive and selective recognition of biomarkers is based on the development of a suitable sensing platform where both molecular recognition (guest-host chemistry) and surface topography can play a pivotal role. In contrast to biological counterparts (enzymes, antibodies and hormone receptors), molecularly imprinted materials display significant advantages, including high mechanical/chemical stability, ease of preparation, potential re-usability, and low manufacturing cost. Simply put, molecularly imprinted polymers (MIPs) are commonly prepared by formation of a three-dimensional polymer network around a template (such as a molecule or an ion) *via* a cross-linking step. The removal of the template creates binding cavities responsible for the recognition process. Such polymers are frequently described as "plastic antibodies" due to their high selectivity. Despite the extensive uses of MIPs in optical, electrochemical, accoustic, piezoelectric and calorimetric sensors, the main challenge still remains regarding the integration of MIP element with various transducers used in sensing devices.[1]

Purine and pyrimidine bases are essential constituents of nucleic acid enzyme cofactors required for the proper functioning of cells, tissues, and organs. Uracil (Ura) is selected in this work as one of the targets from the group of pyrimidines. Ura is involved in the biosynthesis of numerous enzymes necessary for cell functions through bonding with riboses and phosphates. The basal plasma concentration of Ura normally ranged from 2.801 to 30.263 ng mL^{-1}. The Ura derivative, 5-fluorouracil (5-FU), is another target analyte which has been reported as anti-tumor and anti-viral agents. As an antineoplastic agent, 5-FU is used for the treatment of the breast and rectum cancers.[2] Concentration of 5-FU in a patient after 5-FU infusion is usually maintained between 13.007 to 130.077 ng mL^{-1}.[3] Besides, overdoses of Ura and its derivatives produce toxic metabolite accumulation that causes neurotoxicity, inducing morbidity and mortality in humans. Therefore, dihydro pyrimidine dehydrogenase (DPD) deficiency with a defect of the pyrimidine degradation pathway is critically important in the clinical diagnosis of Ura because this is directly associated with the several inborn errors of metabolism. The severe toxicity owing to 5-FU, usually administered as antitumor chemotherapy agent, is also found in DPD-deficient patients.[2] Therefore, in order to obtain information for therapeutic monitoring and scientific research, the development of a practical, reliable and rapid analytical method for highly sensitive determination of ultratrace level of diluted plasma

concentration of Ura and 5-FU is an important analytical agenda. Such study is also warranted to improve the chemotherapy and predict side effects from Ura/5-FU remains in the human body.

Several non-MIP analytical methods such as spectrophotometry, chromatography, capillary electrophoresis, microbiological assays, solid phase extraction, voltammetry and fluorescence have been reported for the Ura/5-FU determination.[2,4-6] However, the cross-reactivity was still crucial with these methods, owing to structural similarity amongst pyrimidine bases prevalent in the real samples. Furthermore, the limits of detection (*LODs)* were found to be insufficient for clinical applications. On the other hand, MIP-based methods were seldom attempted for Ura/5-FU and the respective *LODs* realized were not sufficient for diseases manifested at an acute level of DPD deficiency.[2] In a recent work, an MIP was synthesized for the recognition of 5-FU by RNA-type (nucleobase pairing) driven molecular imprinting.[7] The corresponding piezoelectric microgravimetry/differential pulse voltammetry/capacitive impedimetry sensors revealed high *LODs* (>0.26 mM) and that still needs a major improvement for chemotherapy assessment. In this context, we have already been able to selectively analyze Ura and 5-FU at trace level, without any cross-reactivity in real samples, using MIP-modified hanging mercury electrode.[8] However, the use of mercury should be avoided owing to environmental hazards. The solid electrode (mercury free) reported by our group for Ura and 5-FU analysis also entails certain shortcomings.[9] Accordingly, silica-MIP composite involved a complicated non-hydrolytic sol-gel in the shape of fiber, wherein the ingress and egress of analyte across the interior core and the external surface of cylindrical fiber were apparently hindered to yield the quantification at lower limits. In order to expand the linearity range of Ura and 5-FU analysis down to extreme ng mL^{-1}(say below 1 ng mL^{-1}) level, we have freshly resorted to explore MIP-nanoarray materials for the modification of sensors. The nanometer dimension of nanoarrays structure could be considered most compatible in transduction of better electrical signal to improve sensitivity, specificity and faster response time. Note that MIP- based nanoarrays development is still in infancy.[10,11] In contrast to the MIP nanowires, which are prepared thermally within the pores of aluminium membrane followed by chemically dissolving alumina, have interconnected overlapped heterogeneous texture,[12] MIP-nanoarrays can be prepared following a similar protocol but with a "brush like" texture mostly vertically tethered to the electrode surface which command a larger surface area (or volume) for unhindered analyte diffusion in between any two MIP bristles.

In this work, we present a simple technique for the development of MIP-nanoarrays imprinted with Ura/5-FU at silver (Ag) electrode base surface (Scheme 1). Accordingly, the Ag wire was

anodized at an optimized low electrical voltage to develop small-bore nanopores. These nanopores were subsequently filled with a prepolymerization mixture [N-acryloyl-2-mercaptobenzamide (functional monomer), Ura or 5-FU (template), ethylene glycol dimethacrylate (cross-linker), azobisisobutyronitrile (AIBN, initiator), and MWCNTs] and subjected to the thermal polymerization. The Ag membrane around MIP nanopores was then removed by chemical dissolution, leaving behind MIP- nanoarrays with template molecule binding sites situated at the surface. This allowed π-π electronic interactions between MWCNTs and aromatic precursors (monomer and template) and self-assembled hydrogen bonded monomer-template complex confined within the nano arrays that provide an unique environment of homogeneously distributed recognition sites to promote sensitivity. The use of Ag is advantageous because of its easier oxidative characteristics even at low voltage that helped developing nanoarrays at its base for an uninterrupted mass transport and channelized electronic transmission.[13]

2. Experimental

2.1 Reagents

Acryloyl chloride (AC) was purchased from Loba Chemie (Mumbai, India). Analytes (Ura and 5-FU) and various solvents dimethylsulfoxide (DMSO), chloroform, acetonitrile (ACN), triethylamine (TEA), ethanol, and methanol used in this work, were obtained from Spectrochem Pvt. Ltd. (Mumbai, India). The initiator AIBN, cross-linker ethylene glycol dimethacrylate (EGDMA), multiwalled carbon nanotubes (MWCNTs, internal diameter 2–6 nm, outer diameter 10–15 nm, length 0.1–10 μm, and purity > 90%), and all interferents, were procured from Aldrich (Steinheim, Germany) and Fluka (Steinheim, Germany). Acryl amide (99.9%) was obtained from Loba Chemie (Mumbai, India) and 2-mercaptobenzoic acid from Sigma-Aldrich (Steinheim, Germany). All other chemicals were of analytical reagent grade and used as such. Borate buffer (disodium tetraborate plus HCl) was used as supporting electrolyte (pH 5.6, ionic strength 0.1 M); the pH of buffer could be varied with the addition of a few drops of either 0.1 M HCl or 0.1 M NaOH, as per requirement. Standard stock solutions of Ura and 5-FU (500 μg mL^{-1}) were prepared using deionized triple-distilled water (conducting range $0.06–0.07\times10^{-6}$ S cm^{-1}) and working solutions of these analytes were made from the stock solution by dilution with water. Human blood plasma was brought from the Institute of Medical Science, Banaras Hindu University (Varanasi, India) in an ice-pack and stored at ~4 ^{0}C. We

have deliberately avoided the pretreatment (deprotenization, ultra filtration, etc.) of blood plasma since this may lead to inaccurate data, particularly with ultra-trace analysis. Instead, dilution of blood sample is recommended to mitigate matrix effect to a larger extent. The pharmaceutical formulations analyzed were Uftoral (contains 224 mg Ura/capsule) as procured from P.V. Pharmaceutical Limited (India), and the injection, 5-oncouracil (1.0 mL contains 250 mg 5-FU) from Glaxo Smithkline Pharmaceutical Limited (India). The sample solutions were delivered with the help of highly précised micropipettes obtained from Top-Tech biomedicals (Varanasi, India).

2.2 Apparatus

Voltammetric measurements were carried out at 25 ± 1 ^{0}C on a portable potentiostat μ-Stat 200 (Drop Sens S.L. Oviedo, Spain), which was connected *via* USB connection to a computer installed with the measurement software Drop View (Drop Sens). Differential pulse anodic stripping voltammetry (DPASV) and cyclic voltammetry (CV) were performed using a three electrode cell assembly consisted of MIP-nanoarrays modified Ag electrode, platinum wire, and Ag/AgCl (3.0 M KCl) as working, counter, and reference electrodes, respectively. However, chronocoulometric measurements were performed with the same electrode assembly using an electrochemical analyzer (CH instruments USA, model 1200 A).

Thermo-gravimetric analysis (TGA) of MIP-template(s) adduct and MIP were carried out with a Perkin Elmer-STA 6000 (USA). Fourier transform infrared (FT-IR) spectra of MIP monolith, prepared exclusively for this purpose, were measured on Varian 3100 FT-IR (USA) spectrometer using KBr thin pellet containing the sample. Morphological images of MIP-nanoarrays developed on Ag surface including bare Ag surface were studied using scanning electron microscope (SEM), JEOL, JSM, Netherland, Model 840 A and atomic force microscope (AFM) (Vecco Instruments Inc., USA) with a nanoscope IIIa SPM controller (Digital Instruments, USA, tapping mode). X-ray photoelectron spectroscopy (XPS) experiments were performed using PHI 5000 Versa Probe-II instrument (FEI Inc., USA) which is equipped with the mono Al Kα X-ray radiation (100.1 W, 100.0 μ, 45.0 ^{0}C, 187.85 eV) as the source of excitation in the chamber.

2.3 Computational design of MIP for Ura/5-FU

Monomer-template self-assembly characteristics should be appropriate to obtain a stable complex (MIP-adduct). For this, the selection of monomer which can complex with the template more readily is crucial. In this work, we have studied as many as three monomers that can complex effectively with the template sought for. In order to explore the binding energies involved toward the formation of complex at molecular level, the molecular model of probable template-monomer complex was established using Gauss view 5.0. Hartree–Fock (HF) computation at the second order Moller-Plesset perturbation (MP2) level with a higher 6-31+G (d, p) basis set, in Gaussian09, was attempted for conformation optimization. The minimum binding energies between the optimized conformations of 1:n (Ura/5-FU:monomer) complexes are listed in Table S1, ESI†. The computation of binding energy (ΔE) values for all possible template–monomer combinations is based on the following equation:

$$\Delta E = E_{(template-monomer)} - E_{(template)} - \Sigma E_{(monomer)} \quad (1)$$

Accordingly, the template-monomer complex revealing maximum -ΔE value is screened as a most-suitable model of the complex, at the molecular level.

2.4 Synthesis of functional monomer

The new monomer, N-acryloyl-2-mercaptobenzamide (AMB), was synthesized in two steps. In first step, a 100 mL round bottomed flask, equipped with a reflux condenser and calcium chloride guard tube, was used in which 2-mercaptobenzoic acid (1.54 g, 0.01mol) was reacted with thionyl chloride (4.0 mL) with intermittent stirring. One or two drops of DMF were also added. The reaction mixture was refluxed on a water-bath for 3 h. The excess thionyl chloride was distilled off. A solid residue of 2-mercapto-benzoyl chloride thus obtained was washed with ethanol and dried in air. In second step, 2-mercapto-benzoylchloride (0.98 g, 5 mmol) and acryl amide (0.5 g, 5 mmol) were separately dissolved in DMF, and mixed together with continuous stirring at room temperature for 12 h. This yielded a white colored solid product (AMB). This product was characterized by elemental and spectral (FT-IR) analyses. [Elemental analysis: calculated (%) for $C_{10}H_9NO_2S$: C=57.95, H=4.38, N=6.76, S=15.47; observed (%) C=56.50, H=3.10, N=6.20, S=14.34]; FT-IR (KBr, cm^{-1}): 3395 (N-H stretch), 1650 (C=O), 1680 (C=O), 2586 (S-H), 1580 (C=C), 1464 (Phenyl ring)].

2.5 Electrode preparation

For the preparation of electrode, the Ag wire (diameter of 0.55 mm, 99.99% purity) was inserted into a Teflon tube, and its protruding tip was mechanically polished with an emery paper (No.400) followed with a fine grained alumina powder (particle size of one picometer diameter). Before the electrochemical measurements, the mirror polished electrode was degreased with alcohol and finally rinsed with water. This was subjected to anodization at an optimized potential 2 V for 120 s **(**Fig. S1, ESI†) in an electrochemical cell, containing 10 ml etching solution of 28% liq. NH_3 mixed with two drops of DMF. During the etching process, the solution was stirred gently. Herein, both the reference electrode (Ag/AgCl, 3.0 M KCl) and counter electrode (Pt foil) were kept away from the to-be-etched silver surface with an interdistance of ~2 mm. This resulted in the development of etched porous surface on Ag wire tip which was washed several times with methanol, rather than directly with water, as a self-guard to protect the structure of etched surface.[14]

2.6 Synthesis of MIP-nanoarrays

The preparation of surface molecularly imprinted size-monodisperse nanoarrays is schematically represented in Scheme 1. For the preparation of MIP-nanoarrays, a prepolymer mixture was made with 0.2 mmol AMB (0.041 g, 800 μL DMSO) and 0.1 mmol template (0.010 g, Ura or 0.013 g, 5-FU, 400 μL DMSO) in the presence of an initiator (AIBN, 5 mg/100 μL DMSO) and a cross-linker (200 μL EGDMA in 100 μL DMSO). About 15 mg MWCNTs was added into the prepolymer mixture and purged with N_2 for 5 min. The resulting mixture (20 μL) was spin coated at the tip of etched nanoporous Ag electrode for 15 s at 2600 rpm. Consequently, the nanopores were filled with the prepolymerization mixture. The free-radical polymerization was then initiated thermally at 70 ^{0}C for 7 h. The silver membrane was subsequently removed by chemical dissolution using 0.1 M HNO_3 for 20 min, leaving behind MIP-adduct nanoarrays. Finally, template molecules were extracted out from MIP-adduct arrays by immersing into ACN–TEA mixture (4:1, v/v) for 30 min (for Ura) and methanol:water (1:1, v/v) for 40 min (for 5-FU), under dynamic condition. The extraction efficiency of eluent depends on several factors, such as type of solvent and the ratio of volumes of organic solvent and additive. In the case of MIP-adduct nanoarrays of Ura, ACN was chosen as an eluting solvent because of its better solubility in ACN exhibiting high elution power. In view of basic

characteristics of Ura, the eluting solvent should be highly basic; and therefore, the extraction ability of ACN could further be improved by increasing pH with the use of an organic additive like TEA. It was found that Ura could completely be eluted from MIP-adduct using a high percentage ACN solvent (ACN-TEA, 4:1, v/v), in the present instance. It might be noted that 5-FU could not be easily extracted in the organic solvent mixture (ACN-TEA). Because of the presence of electronegative fluorine atom at C (5) position, 5-FU assumes partially ionized form that requires a polar solvent for the complete extraction; methanol: water (1:1, v/v) was found to be most appropriate one to evolve an ion-pair medium [CH_3O^- H_3O^+] for the complete retrieval of 5-FU from its respective MIP-adduct nanoarrays. Furthermore, 50% aqueous methanol is competent to impart a hydrophilic character to MIP-receptor cleft, wherein H-bondings between MIP and template were fully disrupted, under the influence of water molecules. The complete removal of either of templates was confirmed until the corresponding voltammetric response was not observed. The imprinting protocol is illustrated in Scheme 2. The above procedure was also adopted to obtain non-imprinted polymer (NIP) nanoarrays, but prepared in the absence of template (Ura or 5-FU) in the prepolymer mixture.

2.7 Voltammetric procedure

Voltammetric measurements of MIP-nanoarrays electrode were performed in a cell containing 10 mL disodium tetraborate (pH 5.6). After blank run, the test analyte solution was introduced to the cell for accumulation, under stirring condition, during 210 s accumulation time (t_{acc}) at -1.2V (accumulation potential, E_{acc}) vs. Ag/AgCl. After 15 s equilibration time, DPASV runs were recorded in the potential range varying from -1.2 to -0.5V, at a scan rate 10 mV s^{-1}, pulse amplitude 25 mV, and pulse width 50 ms for both the analytes. Since dissolved oxygen did not affect the stripping current, de-aeration of the cell content was not required. The CV experiments were performed within the potential window -1.2 to -0.2V (with respect to Ag/AgCl) at various scan rates (10-500 mVs^{-1}) in anodic stripping mode. All DPASV runs for each concentration of test analyte were quantified using the method of standard addition. Voltammetric measurements as mentioned above were also performed with the NIP-nanoarrays electrode, under identical operating conditions.

3. Results and discussion

3.1 Theoretical selection of functional monomer and template-monomer stoichiometry

For the template screening, as many as three monomers, *viz*; AMB, 1-acryloyl pyrrolidine-2, 5-dione (APD), 1-(4-hydroxyphenyl) pyrrole-2, 5-dione (HPP) were investigated. Table S1, ESI† lists binding energies of stable complexes of Ura and 5-FU, respectively, with each monomers taken in molar ratios of 1:1 and 1:2. The binding energies were calculated on the basis of optimized conformations of the complexes (Table S1). In principle, a monomer requiring the lowest minimum binding energy (i.e., the highest negative ΔE) would interact strongly with template to form the complex. Evidently from Table S1, Ura and 5-FU interact most strongly with AMB than other monomers (APD and HPP) and moreover, their complexes (1:2) possess the highest negative binding energies. Therefore, MIPs synthesized with AMB_2 is expected to respond the highest binding capacity for either of the analytes understudy.

The aforementioned stoichiometry of the template-monomer complex (1:2) was corroborated on the basis of an empirical equation[15]

$$\frac{1}{i_p} = \frac{1}{i_p.max} + \frac{1}{i_p.\, max\, \beta\, C_t^m} \qquad (2)$$

where, i_p is the measured DPASV peak current, $i_{p,max}$ the peak current when all template molecules formed complex with monomeric precursor, C_t is the concentration of template, m is the coordination number of the complex formed between template and monomer, and β is the stability constant. Substituting m = 1, 2, 3 and 4 in the above equation, the respective $1/i_p$ *vs* $1/C_t^m$ plots showed linearity with the coefficient of variation (R^2) 0.95, 0.99, 0.98 and 0.97, respectively for Ura. Similarly for 5-FU, substituting m = 1, 2, 3 and 4 in the above equation, the respective $1/i_p$ *vs* $1/C_t^m$ plots showed linearity with the coefficient of variation (R^2) 0.98, 0.99, 0.98 and 0.96, respectively. Thus m = 2 can be accepted as a perfect straight line with R^2 = 0.99 for ascertaining template-monomer stoichiometry as 1:2 for both the analytes.

3.2 Polymer characteristics

In the prepolymer solution the amount of different components ought to be optimized to respond the maximum development of DPASV signal. In this work, different template-monomer molar ratios (1:1, 1:2, 1:3, and 1:4) were investigated. It was found that the maximum DPASV response was obtained for any concentration of both analytes when template-monomer molar ratio was 1:2. The decrease in current response with the increase of monomer concentration (say 1:3 and 1:4) may be

attributed to the restricted through-flow owing to the probable steric overcrowdings in the receptor clefts and that also might exert some non-specific binding. On the other hand, the electrode prepared with a unimolar (template: monomer) composition might have inadequate number of binding sites that revealed a poor and non-quantifiable response. It was observed in this work that the best binding affinity between the template and monomer was feasible exclusively with MIP (1:2) under compliance with the concept of stoichiometric non-covalent interactions between them. Insofar as an optimized amount of cross-linker (monomer: EGDMA molar ratios 1:1, 1:5, 1:10, 1:15, and 1:20) for MIP development is concerned, this should be a typical amount of cross-linker that can control MIP flexibility so as to accommodate template into its cavity, without any hindrance. Accordingly, the monomer-crosslinker ratio of 1:5 was found to be best one to obtain maximum current, for any concentration of both the analytes. Any amount of cross-linker higher than this (>5 mol) might produce sterically hindered cross-linked network affecting the analyte diffusion. In all electrodes, as much as 15.0 mg MWCNTs was required to enhance the membrane electro-conductivity; excess amount (>15.0 mg) of MWCMTs revealed a drastic curtailment of DPASV response presumably due to MWCNTs flocculent texture causing heterogeneity in the MIP membrane. Other parameters such as polymerization time and polymerization temperature have major impact on MIP synthesis, and thereby the sensor response. The polymerization time of 7 h and temperature 70 ^{0}C were found to be optimum for responding the maximum DPASV current (Fig. S1, ESI†).

3.3 Spectral characterization

FT-IR (KBr) spectra of the templates (5-FU and Ura), their MIP-adducts, and MIP (template-free), as synthesized separately in bulk, were comparatively studied (Fig. S2, ESI†). Accordingly, typical bands of the 5-FU [N_1 (H), 3131 cm^{-1}; N_3 (H), 3069 cm^{-1}; C_2 (O), 1690 cm^{-1}; C_4 (O) stretch, 1730 cm^{-1}; and CN stretch, 1430 cm^{-1}] are shifted downward to 3063, 2980, 1640, 1670 and 1390 cm^{-1}, respectively. The vibrational bands of Ura [N_1 (H), 3440 cm^{-1}; N_3 (H), 3380 cm^{-1}; C_2 (O), 1645 cm^{-1}; C_4 (O), 1716 cm^{-1}] are also downward shifted to 3300, 3250, 1637 and 1675 cm^{-1}, respectively. Besides, the respective bands of monomer [1682 cm^{-1} (-C=O stretch), 1660 and 959 cm^{-1} (amide II band)] are found to be shifted to 1655, 1510 and 880 cm^{-1}, upon complexation with both analytes. Consequently one may predict four-point hydrogen bonding interactions between template and monomer as shown in Scheme 2. It may be further noted that all shifted bands of both templates disappeared and monomer bands reinstated at their original positions, upon template retrieval. This

indicates the complete extraction of the template molecules from their corresponding molecular cavities. Note that the N-H stretching amide bands of Ura and 5-FU are found to be usually very weak. These bonds however, turned to be broader under the influence of their hydrogen bondings with the polymer receptor cleft. The weak C-F bands with 5-FU (Fig. S2A) and MIP-5-FU adduct (Fig. S2C) are observed at same position (around 1500 cm^{-1}), suggesting no interaction of this functionality in self assembling of monomer-template complexation. The presence of MWCNTs in all polymer motifs might also be revealed from aromatic C-N out-of-plane weaker bending in the low frequency range between 800 and 600 cm^{-1}.

XPS (Fig. 1A-D) was used to investigate the composition of coating materials such as MIP-Ura-adduct, MIP-5-FU adduct, and their corresponding MIPs. Accordingly, both types of film indicate two sharp peaks of C1s and O1s, including a feeble peak of N1s. The feeble peak of N1s present in either MIP-template adduct or MIP may be accorded with its atomic percentage as low as 1.4-0.4%. Interestingly, the characteristic F1s (atomic concentration 0.4%) feeble peak at about 700 eV of template (5-FU) in MIP-adduct (Fig. 1C) is found to be conspicuously absent in corresponding MIP motif (Fig. 1D). This indicates the complete retrieval of 5-FU from MIP-adduct.

The fitted (deconvoluted) O1s (30.5-31.0%), N1s (1.4-0.4%), C1s (68.7%) XPS spectra of MIP-adduct (Ura/5-FU) are shown in (Fig. 2A-F). Fig. 2 (A and D) depicts two peaks at 530.6 and 532.1 eV corresponding to -C=O and -C-O, respectively. Fig. 2 (B and E) displays only one peak at 398.4 eV for N1s. Fig. 2 (C and F) consists of three peaks at 283.6, 285.2, and 287.6 eV which may be attributed to C=C/-C-C, -C-N and –C=O groups, respectively. An additional peak corresponding to -C-F group is observed with MIP–5-FU-adduct (Fig. 2F). A large number of C=C and C-C bonds prevalent on the film reflect the potential of embedded MWCNTs to adsorb target analyte(s) by π-π interactions. Similar pattern of peaks are observed with MIP/NIP coatings (Fig. S3A-F, ESI†). A close perusal of MIP system, the C1s binding energy is about 284.68 eV for MIP (Ura) and 284.73 for MIP (5-FU) corresponding to –C-N which increases to 285.26 and 285.21 eV, respectively upon H-bonding as –C-N--H. The O1s also increases from 531.98 to 532.14 to reflect the covalency of the –C-O--H bond.[16] There was no significant change in the N1s peak with template adsorption as it is routinely detected at about 398.4 eV. The deconvoluted spectra of MIP/MIP- adduct further reveal the fact that the nitrogen peak intensity of MIP-adduct coating is decreased when template molecules are removed to obtain MIP film. The decreased nitrogen peak is almost equivalent to that of NIP coating (Fig. S3E). The peak area 226.52 (MIP-Ura adduct) and 155.14 (MIP-5-FU adduct) of N1s (a.u.) is

decreased to 71.43 and 71.66, respectively upon template retrieval. Interestingly, this decreased peak area, which corresponds to N1s of MIP film, is close to N1s peak area (69.90) observed with NIP coated surface. In the similar tune, the atomic concentration (1.4%) of nitrogen of MIP-adduct has also been found to be decreased to 0.4% on both MIP and NIP modified surfaces, this suggested a complete template (Ura/5-FU) retrieval from MIP-adduct. The nature of adsorption of template (Ura/5-FU) on MIP with the formation of critical hydrogen bonds is still somewhat ambiguous in XPS as no significant shifts in XPS binding energies of key elements (O, N, C) with template adsorption are observed. Because the O1s and C1s signals were so strong in MIP, shoulder peaks from the expected surface oriented template molecules were found to be obscured by the stronger peaks of a large number of –C=C, C-C, and –C=O groups prevailed on the surface of the MIP receptor cleft. Nevertheless, FT-IR analysis gave strong indications that hydrogen bonding to the MIP surface had occurred in the present investigation.

3.4 Morphological characterization

The bare Ag surface showed a smooth SEM image (Fig. 3A) which, however, turned into nanopores upon anodization at 2 V (Fig. 3B). These pores were filled-in by MIP-adduct and appeared to possess a similar texture for both analytes (Fig. 3C). Upon template retrieval one may clearly visualize uniformly dispersed carbon nanotubes in proximity with nanoarrays. Herein, MWCNTs imparted a highly specific and large surface area to the entire texture for an effective adsorption of aromatic molecules through π-π cooperative interactions (Fig. 3 D and F). Interestingly, the diameters of MIP-nanoarrays (Fig. 3D for Ura and Fig. 3E for 5-FU) are observed to be 60 nm which is in tune with the nanopore size developed on the silver surface. Notably, the size of polymer nanoarrays could be controlled by changing the pore size on silver surface at different potentials. These nanoarrays were vertically aligned over the substrate surface, even after chemical dissolution of silver and probable mechanical relaxation in the polymer texture. The side image (72935× magnification) of MIP-nanoarrays layer on the electrode revealed the coating thickness to be 86.9 nm (Fig. 3F).

Surface morphologies are further examined using AFM two dimensional images (Fig. 4A-C). The arithmetic mean roughness (*Ra*), root mean square roughness (*Rq),* and the surface height *(Rz*) for MIP-adduct with both templates are observed to be 62.6, 77.5, and 405.6 nm, respectively. On the other hand, after templates (Ura/5-FU) removal, the *Ra, Rq* and *Rz* values are obtained to be 77.2, 85.3 and 376.4 nm, respectively. The increase of surface height on adduct formation vis-à-vis

imprinted polymer reflects a template embedded structure. An average thickness of imprinted nano-arrays surface for Ura/5-FU was estimated using the following equation:[17]

$$z(x,y) = s(x,y) + t + \Delta z(x,y) \quad (3)$$

where, *z(x, y)* is the surface-height (376.4 nm) of imprinted nanoarray electrode, *s(x, y)* is the surface-height (199.3 nm) of bare Ag electrode, t is the average thickness, and *Δz (x, y)* is the inherent roughness *(Rq* = 85.3 nm) of imprinted electrode for Ura/5-FU. The calculated value of mean thickness (*t*) of coating was found to be 91.5 nm in close approximation with that obtained by SEM.

3.5 Electrochemical behavior

Preliminary CV experiments were performed for both analytes Ura (Fig. 5A) and 5-FU (Fig. 5B) using their respective MIP-nanoarrays electrodes. For both analytes, CV experiments show the emergence of two peaks (I and II). Peak II appears as post-adsorption wave due to the physisorbed phase of Ura/5-FU at the electrode surface. The post-adsorption peak (II) remains constant at higher concentration (>5.44 ng mL^{-1}) but not distinguishable at lower concentration of analyte (<1.42 ng mL^{-1}). On the other hand, peak I was irreversible at the lower scan rates (≤20 mV s^{-1}). Latter, the peak I has developed a tendency to be quasi-reversible at higher scan rates (>20 mV s^{-1}, E_{pa}-E_{pc} >100 mV s^{-1}, i_{pa}/i_{pc} >1) presumably due to insufficient time given to cathodic reduction in the reverse scan. The restricted cathodic peak owing to the reduction of oxidation product (neutral free radical under pool of electrostatic interaction with positively charged electrode) may also involve its weak adsorption on the electrode surface to some extent without revealing any emergence of pre-peak in anodic scan. The oxidation potential of 5-FU (-0.80 V) is lower than that of Ura (-0.75 V); the electro-activity of 5-FU is rather facilitated, owing to the substitution of electron-withdrawing fluorine at C (5) position, as compared to Ura. As reported earlier,[9] the oxidative electron reaction involved -1e^{-}, -1H^{+} process to produce a free-radical form of oxidation product (Scheme 2, Inset). This mechanism is most plausible to comprehend the higher electro-activity of 5-FU than that of Ura. Accordingly, both analytes are initially oxidized at anode to lose one electron from N (1) to form cationic intermediate, followed by de-protonation at the N (1) to produce a possible neutral free radical. Replacement of hydrogen of Ura by an electron-withdrawing fluorine atom at C (5) might enhance the de-protonation at N (1) via decreasing the charge intensity of N (1) and subsequently, the free radical becomes more stabilized due to resonance stabilization. This could be a driving force to

augment the electro-activity of 5-FU that apparently required a lower energy for electro-oxidation, with as much as 50 mV difference on the CV and DPASV potentials between Ura and 5-FU. In present case, both analytes have shown irreversible electron transfer at lower scan rate ≤20 mV s^{-1} because of the fact that the free radical might have trapped in the pool of aromatic rings (AMB residues) of the surrounding cavity in the sufficient time scale of voltammetry. Such action appears to be insufficient at >20 mV s^{-1}; and hence, the electron process in the reverse scan attained to a quasi-reversible nature. As predicted by the linear profiles of E_{pa} *vs* log ν and i_{pa} *vs* $\nu^{1/2}$, both analytes underwent anodic stripping under diffusion-controlled process. The quasi-reversibility was further confirmed from different slopes of i_{pa} *vs* $\nu^{1/2}$ and i_{pc} *vs* $\nu^{1/2}$ profiles as shown below:

Ura;

$I_{pa} = (-15.303 \pm 2.321) + (128.119 \pm 6.140)\ \nu^{1/2}$ $R^2 = 0.99$ (4)

$I_{pc} = (-3.166 \pm 0.582) + (16.836 \pm 1.280)\ \nu^{1/2}$ $R^2 = 0.98$ (5)

5-FU;

$I_{pa} = (-13.246 \pm 2.560) + (109.072 \pm 6.771)\ \nu^{1/2}$ $R^2 = 0.98$ (6)

$I_{pc} = (-6.005 \pm 1.398) + (31.775 \pm 3.074)\ \nu^{1/2}$ $R^2 = 0.98$ (7)

We have also explored the electrode kinetics in this work under the prevailing condition of quasi-reversibility as discussed elsewhere.[18] Accordingly, ΔE_p values were introduced in the working curve described by Nicholson for obtaining the electron transfer parameter, ψ, and then the value of K^0 was estimated according to the following equation:

$$\psi = \frac{K^0 (D_{oxi}/D_{red})^{\alpha/2}}{(\pi D_{oxi} n F \upsilon / RT)^{1/2}} \quad (8)$$

To estimate K^0 from Eq. (8), the diffusion coefficient (assuming $D_{oxi} = D_{red} = D$) was obtained from the chronocoulometry experiment. According to the integrated Cottrell equation, the relationship between Q and $t^{1/2}$ (Anson plots) can be described as follows:

$$Q_{total} = Q_{dl} + Q_{ads} + Q_{diff} \quad (9)$$

$$Q_{total} = 2nFAC(Dt)^{1/2}\,\pi^{-1/2} + Q_{dl} + Q_{ads} \quad (10)$$

$$Q_{ads} = nFA\Gamma^0 \quad (11)$$

where, A is the real electrochemical surface area of three dimensional nanometric structure coated on the working electrode (A=0.20 cm^2), C is the concentration of analyte (20 ng mL^{-1} Ura/5-FU), Q_{dl} the double layer charge, Q_{ads} the Faradic oxidative charge, n the number of electron and Γ^0 is the surface coverage. For the determination of A, the Randles-Sevick equation (Eq. 12) could be better than that obtained with any ordinary tool (designed to measure the radius), because the latter estimates the geometrical surface area (A_{geom}=0.0023 cm^2). Accordingly, the peak current at 25 ^{0}C, for A in cm^2, D in cm^2 s^{-1}, C^0 in mole cm^{-3}, and v in V s^{-1}, I_p in amperes, is

$$I_p = (2.687 \times 10^5) n^{3/2} A D^{1/2} v^{1/2} C^0 \quad (12)$$

where, D represents diffusion coefficient (0.76 x 10^{-5} cm^2 s^{-1}) of ferricyanide used as a mediator probe; other parameters have their usual meanings and Γ^0 is the surface coverage (mol cm^{-2}). For MIP-sensor, Q_{dl} and total charge (Q_{dl} +Q_{ads}) can be estimated from the intercepts of the Anson plots of charge (Q) vs. square-root of time ($t^{1/2}$), in the absence and presence of analyte, respectively. The difference between these intercepts is Q_{ads} (for Ura: Q_{ads} = 1.43×10^{-5} μC and for 5-FU: Q_{ads} = 1.36×10^{-5} μC). In order to determine the Γ^0, it is necessary to find 'n'. The 'n' value can be calculated by applying an empirical equation defining Nerstian adsorbent layer:

$$I_{pa} = [\frac{n^2 F^2}{4RT}] \Gamma^0 A v \quad (13)$$

and that was found to be equal to 1.09 for Ura and 0.98 for 5-FU. Finally, substituting the value of n in Eq.13, Γ^0 values are calculated as 0.6715×10^{-9} and 0.7109×10^{-9} mol cm^{-2} for Ura and 5-FU respectively. Therefore, the total electrode surface was covered by 1.363×10^{-10} mol (8.211×10^{13} molecules) of Ura and 1.443×10^{-10} mol (8.6925×10^{13} molecules) of 5-FU; each molecule in both cases occupied one molecular cavity of their respective MIPs. Such large number of Ura/5-FU molecules were easily accommodated on the enhanced surface area (A = 0.20 cm^2) of the electrode apparently due to its MIP-nanoarrays surface coverage. Furthermore, from the slopes (3.17×10^{-4} μC s^{-1} for Ura and 3.29×10^{-4} μC s^{-1} for 5-FU) of the Anson plots, diffusion coefficients (D) were also calculated as 5.318×10^{-3} and 9.678×10^{-3} cm^2 s^{-1} for Ura and 5-FU, respectively. The diffusion coefficients reported for 5-FU and Ura were 4.84×10^{-4} and 2.04×10^{-4} cm^2 s^{-1}, respectively realized on traditional MIP fiber modified electrode.[9] The diffusion coefficients realized in the present work for both analytes are approximately 10-fold higher. This suggests a relatively high diffusion kinetics

allowing unhindered mass-transfer of analyte across vertically tethered bristles of MIP-nanoarrays as compared to standard MIP film. The analyte diffusion within nanoarrays, arranged as MIP brush, is facilitated through upward motion (vertical diffusion), in contrast to the longitudinal diffusion on MIP-fibers/film. This could be considered advantageous to augment the sensitivity of the measurement with nanoarrays vis-a-vis nanofibers or solid thin film. Substituting the D value ($D_{oxi} = D_{red}$), K^0 values at different scan rates were calculated for Ura from Eq. (8) for different values of ψ [0.45 (50 mV s^{-1}), 0.30 (100 mV s^{-1}), 0.20 (200 mV s^{-1}), 0.12 (500 mV s^{-1})] as 2.67, 2.49, 2.38 and 2.25 cm s^{-1} (mean K^0= 2.44 cm s^{-1}). Similarly, K^0 values calculated for 5-FU were obtained as 6.85, 4.84, 4.26 and 4.81cm s^{-1} (mean K^0= 5.19 cm s^{-1}). The decrease in K^0 represents sluggish kinetics of electron-transport for Ura/5-FU oxidation with the increase of scan rate, under the adsorbed state of analyte in the domain of molecular cavities of imprinted polymer.

3.6 Analyte adsorption behavior

Despite the fact that the NIP had many hydrogen bonding moieties, the corresponding nanoarrays are compact and devoid of any molecular cavity, in absence of print molecules. The vertically tethered NIP bristles, though allows faster mass transport through any two proximate bristles from downward (brush tip) to upward (electrode base), the contact (retention) time is consequently reduced to effect any significant analyte adsorption. On the other hand, the similar analyte diffusion within the two MIP-bristles might cause selective retention of analyte molecule into the corresponding pockets (cavities) under the influence of imprinting effect. The analyte adsorption insignificantly realized on NIP nanoarrays was non-specific which includes some adsorption of Ura and 5-FU onto MWCNTs via π-π interactions. Fortuitously, such non-specific adsorption could be curtailed simply by water-washings and MIP sensor should also be given the similar washing treatment, as a safeguard, to avoid any false-positive contribution before DPASV measurements.

Selective adsorption of test analyte(s) from bulk to their respective MIP cavities could be approximated on the basis of the Langmuir equation:[18]

$$\frac{C}{\Gamma^0} = \frac{1}{B_{ads}\,\Gamma^{max}} + \frac{C}{\Gamma^{max}} \qquad (14)$$

where, B_{ads} is the adsorption coefficient and Γ^{max} the maximum amount of analyte that can adsorb on the surface. In this work, a linear equation, C/Γ^0= (892.1549 ± 77.745) × 10^6 C + (198.91 ± 44.127) (R^2 = 0.98), for the plot of C/Γ° vs. C is obtained for Ura. Accordingly, the intercept (equivalent to

slope/B_{ads}) of this equation gives an estimate of the adsorption coefficient (B_{ads}) equal to 4.5031×10^6 L mol^{-1}. Similarly, $C/\Gamma^0 = (520.633 \pm 56.16) \times10^6\, C + (151.41 \pm 27.51)$ ($R^2 = 0.97$) for 5-FU revealed B_{ads} as 3.438×10^6 L mol^{-1}. The Gibbs free energy change ($\Delta G = -RT\, ln\, B_{ads}$) due to analyte adsorption could be calculated as - 37.963 and -37.295 kJ mol^{-1} for Ura and 5-FU, respectively. The large negative value of ΔG_{ads} indicates spontaneous analyte adsorption on their MIP-nanoarrays.

3.7 Optimization of analytical parameters and analytical determination

Operating conditions for DPASV measurement were optimized for pH, accumulation potential (E_{acc}) and accumulation time (t_{acc}). The supporting electrolyte (disodium tetraborate solution, 0.1 M ionic strength) pH had major impact on the oxidation of 5-FU/Ura. The maximum development of DPASV current was reached at pH 5.6 (despite the fact that pK_a H_3BO_3 = 9.24); any pH higher than this registered a sharp fall in 5-FU/Ura current (Fig. S4, ESI†). This may be due to dianionic formation (lactim form) of pyrimidine at pH≥7.0 with restricted accumulation under electrostatic repulsion forces operating between electrode and electrolyte. The peak potential (E_p) was found to shift negatively following linear equations.

For Ura;

$$E_p\,(\mathrm{V}) = (-0.0573 \pm 0.005)\ \mathrm{pH} + (0.42 \pm 0.03) \qquad R^2 = 0.977 \qquad (15)$$

For 5-FU;

$$E_p\,(\mathrm{V}) = (-0.0591 \pm 0.005)\ \mathrm{pH} + (0.45 \pm 0.037) \qquad R^2 = 0.975 \qquad (16)$$

The slope values of the above equations thus corroborate the participation of equal number of electron and proton ($1e^-$, $1H^+$) in the electrode reactions for both analytes. The analyte (5-FU/Ura) accumulation at the electrode surface was optimum at highly negative potential (E_{acc} = -1.2 V) because of substantive hydrophobically induced rebinding of the analyte through hydrogen bondings in the hydrophobic domains of cavities. Notably, optimum t_{acc} of the 5-FU/Ura was 210 s; thereafter a saturation of binding sites has been occurred to respond a constant current. When all the operating parameters were optimized, the DPASV determinations of 5-FU and Ura were carried out. Fig. 6, shows the DPASV measurements on MIP-nanoarrays electrode in the aqueous samples (Fig. 6A for Ura and 6B for 5-FU). The most attractive feature of nanoarray electrodes was the development of highly symmetrical DPASV peaks in complicated matrices like blood plasma and pharmaceutical samples. A series of various aqueous and real samples for both 5-FU and Ura were investigated using

DPASV under optimized operating conditions on the respective MIP-nanoarrays electrodes. The corresponding linear regression equations (I_p *vs.* C), correlation coefficients (R^2), recoveries, and *LODs*, are portrayed in Table 1. A complete saturation of binding sites occurred at 401.5 and 278.7 ng mL^{-1} for 5-FU and Ura, respectively; corresponding NIP-modified electrodes did not respond any current below these concentrations. This indicates the absence of any non-specific adsorption on MIP-nanoarrays electrode up to the level of maximum analyte binding. Thus, all data in this work are without false-positive contributions. The proposed method is compared with an MIP-composite fiber electrode,[9] by means of student's t-test (t_{cal} 2.13 < t_{tab} 2.77 for Ura and t_{cal} 2.35 < t_{tab} 2.77 for 5-FU, confidence level 95%, R^2 = 0.99) in the lower concentration regions (Ura: 2.58–9.91 ng mL^{-1} and 5-FU: 13.88–22.72 ng mL^{-1}) in blood plasma samples. Although both methods are highly précised, the sensitivity of proposed sensor is somewhat superior than earlier work [*LOD*; 2.12 ng mL^{-1} for 5-FU and 0.64 ng mL^{-1} for Ura].[9] On the other hand, the proposed sensor is relatively cost-effective, portable, and easy-to-use with high sensitivity for disease diagnosis in clinical settings, without any false-positive or cross-reactivity. It is worth to compare the proposed MIP sensor with other known methods for the determination of Ura and 5-FU (Table S2, ESI†). Accordingly, the proposed sensor is capable for Ura/5-FU analysis in real samples without any matrix effect and cross-interferences; the most of the earlier work (barring our work) were not properly validated either with real samples or in the presence of interferents.

3.8 Selectivity of the sensor

In order to verify the recognition-selectivity of the imprinted sensor with the template(s), we have studied the electrochemical response of MIP and NIP electrodes for many purine and pyrimidine bases, viz., adenine (Ade), guanine (Gua), cytosine (Cyt), thymine (Thy), and some other biologically important molecules viz., dopamine (DA), hypoxanthine (Hypo), barbituric acid (BA), ascorbic acid (AA), caffeine (Caff), uric acid (UA), creatine (Cret), urea, glucose (Glu) and their clinically relevant mixture. Accordingly, MIP-modified electrode was not responsive for any of the interferents when studied individually. On the other hand, the NIP modified electrode revealed very feeble current response for some of the interferents (Fig. S5A, ESI†), which could easily be washed away from the electrode with water (n = 3, 1.0 mL). This confirmed a substrate selective imprinting effect in this case. The parallel cross-reactivity study (Fig. S5B, ESI†) has also been made in the binary mixture of interferents and test analyte (clinically relevant concentration ratio). Herein, the MIP-modified

electrode showed quantitative (100%) response for Ura/5-FU. This suggests that the sensor can also be used for the quantitative analysis of Ura/5-FU in the sample containing very high concentration of interferents. From this experiment it can easily be surmised that the MIP binding sites present at the MIP surface are able to recognize Ura/5-FU molecule, in the presence of any concentration of interferents, by means of stereochemical selectivity in terms of shape, size, and chemical affinity of the functional groups.

When the analyte and interferents (each 19.607 ng mL^{-1}) were studied individually, without undergoing water-washings, after adsorption on MIP-Ura/5-FU modified nanoarrays silver electrode and corresponding NIP modified nanoarray electrode, the selectivity coefficient (k) and relative selective coefficient (k') values were obtained as

$$k = \frac{i_{interferent}}{i_{sample}} \quad (17)$$

$$k' = \frac{k_{MIP}}{k_{NIP}} \quad (18)$$

where $i_{interferent}$ is the current response of interfering material solution, i_{sample} is the current response of sample solution, k_{MIP} and k_{NIP} are selective coefficients for MIP and NIP, respectively. The k and k' values for Ura and 5-FU with respect to interferents/ structural analogues are summarized in Table 2. Almost no interference (<0.3%) was observed with all the interferents on MIP and NIP sensors. The reason could be based on the fact that interferents like Ade, Gua, DA, Hypo, Caff, UA, and Glu, are bigger than Ura/5-FU in molecular size and cannot enter into the imprinting sites of the MIP nanoarrays. On the other hand, the structurally identical interferents like Cyt, Thy, BA, AA, and Cret, and smaller molecule like urea have a fair chance of approaching the imprinting sites but still mismatch the imprinting sites for binding. The results for k' for both analytes, showing selectivity gained by imprinting process, display that the imprinted sensors have perfect selectivity [MIP (Ura) : 159 times more selective than 5-FU, MIP (5-FU) : 1100 times more selective than Ura] with imprinting factor (*I.F.* = i_{MIP}/i_{NIP}) for both template (Ura and 5-FU) as high as 67 and 77, respectively. This reflects an excellent imprinting phenomenon in this study.

3.9 Reproducibility and stability

To explore reproducibility and ruggedness of the proposed sensor, multiple DPASV runs were recorded for both the analytes Ura and 5-FU (each 29.56 ng mL^{-1}). The relative standard deviation (*RSD*) for the same sensor was about 1.12%. To evaluate electrode to electrode reproducibility, a

series of as many as five modified electrodes were prepared in the same way and tested for 29.56 ng mL^{-1} 5-FU. All electrodes responded quantitatively (100%) with *RSD* 0.63%. Regeneration of the modified electrode, after each DPASV measurement, could be feasible employing the reported method of template retrieval, i.e., using respective eluents in dynamic condition. Current intensities of analyte decreased to 3.18% of the initial value after being used more than 45 rebinding/extraction cycles. Insofar, as exposure to the extractant (ACN:TEA, 4:1, v/v, for Ura, and methanol:water, 1:1, v/v, for 5-FU) for recycling of MIP-nanoarrays is concerned, the proposed sensor for both analytes were found to be chemically stable at the working pH (5.6) and temperature (25^0C), without showing any deviance in DPASV response upto 45 regeneration cycles. The stability of the proposed sensor was also examined by intermittent measuring of DPASV response to standard Ura solution, on every third day, over the period of one month. A similar conclusion could be withdrawn when MIP-Ura electrode reproducibility and ruggedness were examined in aqueous and real environments. This demonstrated that the prepared electrochemical sensor had excellent regeneration and ruggedness claiming, a novel class of MIP-nanoarrays electrodes for Ura/5-FU sensing at ultratrace level.

Thermal stabilities of MIP-Ura and MIP-5FU sensors are impressive in the sense that the respective imprinted polymer was found to be stable at upto as high as 190^0C (with minor weight loss of moisture) as revealed by TGA (Fig. S6, ESI†). As evinced from TGA curves, MIP degradation (curve a) proceeds with the gradual weight loss in temperature ranges: 30-85^0C, 190-450^0C and 460-640^0C, corresponding to three successive weight losses of 0.26%, 95.97% and 2.48%. The degradation pattern may tentatively be assigned due to water loss, monomer and crosslinker degradations. Interestingly, as many as four successive weight losses for MIP-template adduct (curve b) are: 30-85^0C, 85-240^0C, 240-450^0C and 460-640^0C corresponding to weight loss of 10.76% (water), 22.35% (template), and 95.97% (monomer) and 2.48% (crosslinker) degradations. The observed weight loss of 22.35% exclusively in second step of TGA curve of MIP-adduct corroborates the calculated loss (23.85%) due to the template degradation from the polymer motif. Since there was no weight loss observed corresponding to template in TGA curve of MIP (Fig. S6a, ESI†), this supports the complete retrieval of template(s) from MIP-template adduct.

4. Conclusions

For the first time, we are reporting MIP-nanoarrays based Ag electrode for Ura/5-FU determination in real samples with detection sensitivity as low as 0.50 ng mL^{-1} for Ura and 0.33 ng mL^{-1} for 5-FU. For

the faster ingress and egress of both analytes, the "surface imprinting" with nanoarrays on silver substrate has been found to be advantageous to render a larger surface area with vertically aligned nanopores for uninterrupted mass-transport and electron-transfer with high kinetics. This investigation demonstrates a phenomenon improvement of our work[8,9] reported for Ura/5-FU analysis, in terms of sensing and therapeutic range of quantification.

Acknowledgments

One of the authors (AK) acknowledges the financial support as Junior Research Fellowship (No. 09/013(0513)/2013-EMR-I) from Council of Scientific and Industrial Research (CSIR), New Delhi India.

Supporting Information

†Electronic Supplementary Information (ESI) available: Figures showing optimizations of polymer composition and analytical parameters, FT-IR, deconvoluted XPS spectra, DPASV response for analyte and interferents, TGA, Tables for binding energies of optimized complexes, and comparison of different methods.

References

1 M. J. Whitcombe, N. Kirsch and I. A. Nicholls, *J. Mol. Recogn.*, 2014, **27**, 297-401.

2 K. Pandey, R. S. Dubey and B. B. Prasad, *Ind J. clin. Biochem*., DOI*:* 10.1007/s12291-015-0482-4.

3 M. Breda and S. Baratte, *Anal. Bional. Chem.*, 2010, **397**, 1191−1201.

4 V. Mirceski, S. Skrzypek and M. Lovric, *Electroanalysis*, 2009, **21**, 87−95.

5 D. Zhu, Y. Chen, L. Jiang, J. Geng, J. Zhang and J. J. Zhu, *Anal. Chem*., 2011, **83**, 9076−9081.

6 M. S. Khot, S. L. Bhattar, G. B. Kolekar and S. R. Patil, *Spectrochim. Acta* A, 2010, **77**, 82−86.

7 T. P. Huynh, P. Pieta, F. D'Souza and W. Kutner, *Anal. Chem.*, 2013, **85**, 8304−8312.

8 B. B. Prasad, S. Srivastava, K. Tiwari and P. S. Sharma, *Sens. Mater.*, 2009, **21**, 291−306.

9 B. B. Prasad, D. Kumar, R. Madhuri and M. P. Tiwari, *Electrochim. Acta*, 2012, **71,** 106– 115.

10 F. Berti, S. Todros, D. Lakshmi, M. J. Whitcombe, I. Chianella, M. Ferroni, S. A. Piletsky, A. P. F. Turner and G. Marrazza, *Biosens. Bioelectron*., 2010, **26**, 497−503.

11 M. S. She and R. M. Ho, *Polymer*, 2012, **53**, 2628−2632.

12 R. Ouyang, J. Lei and H. Ju, *Chem. Commun*., 2008, 5761–5763.

13 B. B. Prasad, R. Madhuri, M. P. Tiwari and P. S. Sharma, *Anal. Chim. Acta*, 2010, **681**, 16–26.

14 C. Fang, A. V. Ellis and N. H. Voelcker, *J. Electroanal. Chem*., 2011, **659**, 151−160.

15 X. Gao, *Handbook on the Physics and Chemistry of Rare Earths*, Elsevier Science Publishers BV, 1986, **8**, pp. 163.

16 G. Beamson and D. Briggs, *High Resolution XPS of Organic Polymers,* Wiley, Chichester, 1992, pp. 295.

17 B. B. Prasad and I. Pandey, *Electrochim. Acta*, 2013, **88**, 24-34.

18 B. B. Prasad, A. Prasad and M. P. Tiwari, *Biosens. Bioelectron.*, 2013, **39**, 236-243.

Figures and Tables

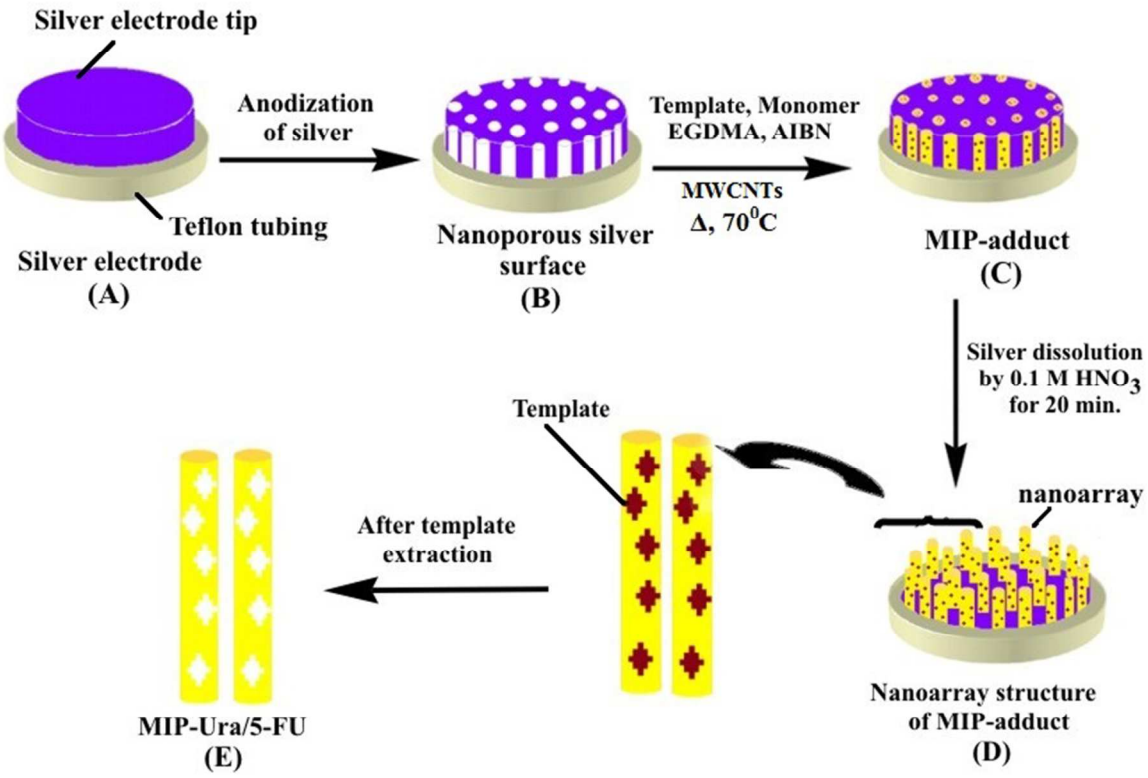

Scheme 1 Schematic representation for the preparation of MIP-nanoarrays onto the silver surface.

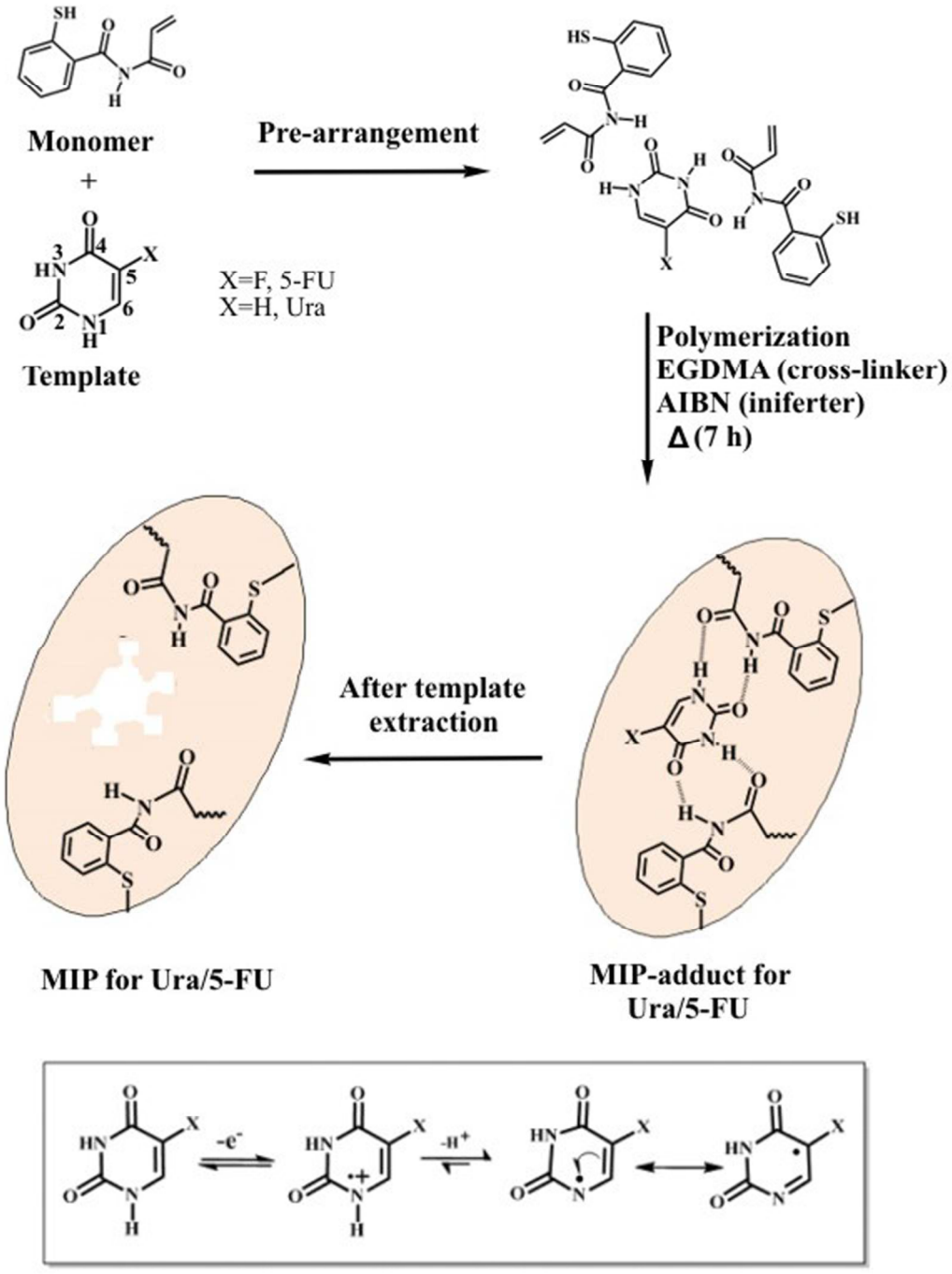

Scheme 2 Binding mechanism of Ura/5-FU in their respective MIP-cavities and electron transfer mechanism (Inset).

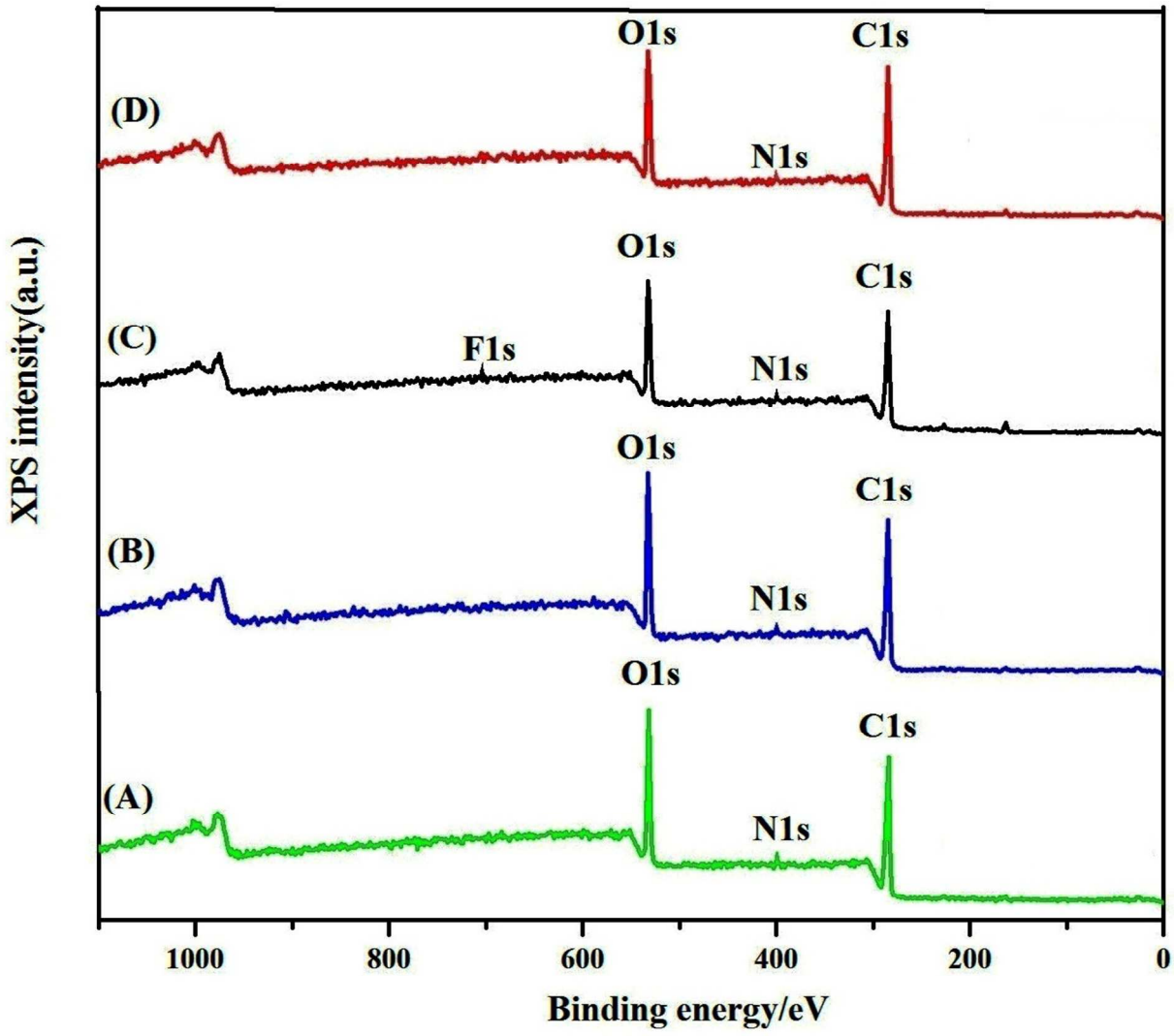

Fig. 1 XPS spectra: (A) MIP-Ura adduct, (B) MIP-Ura, (C) MIP-5-FU adduct, and (D) MIP-5-FU

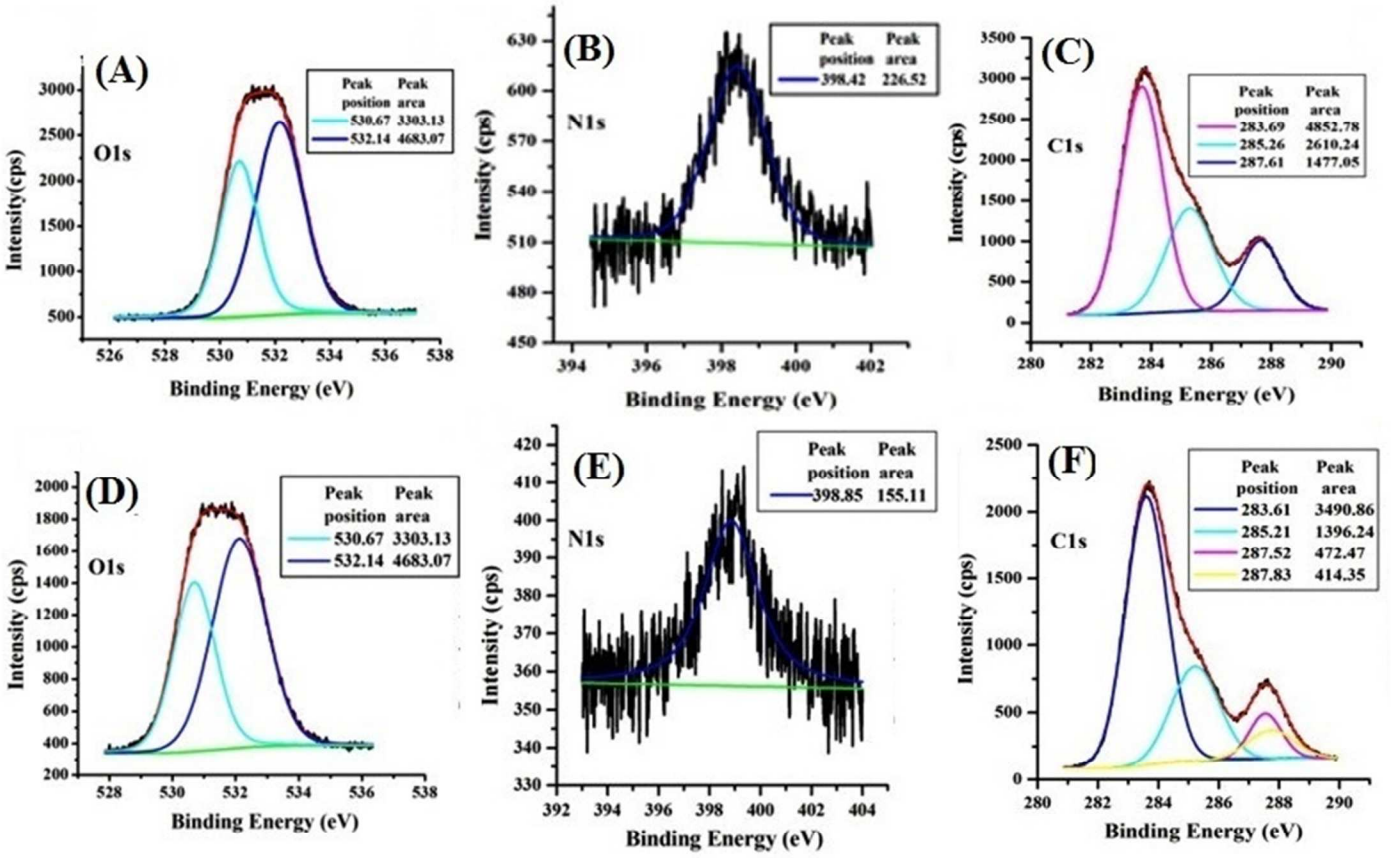

Fig. **2** Deconvoluted XPS spectra of various elements of MIP-Ura adduct (A-C) and MIP-5-FU adduct (D-F).

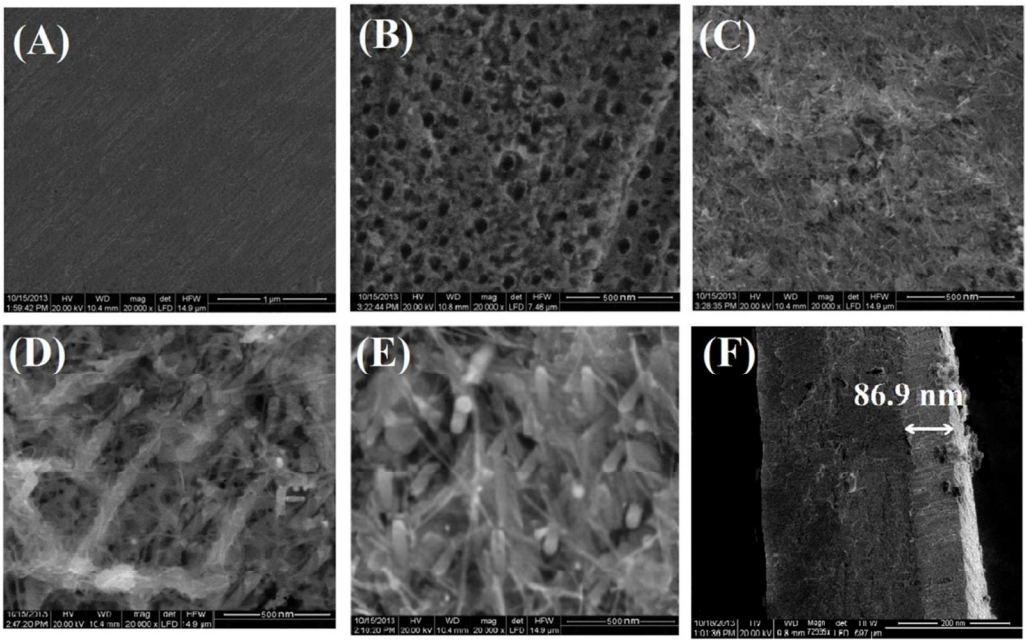

Fig. 3 SEM images: (A) bare silver surface, (B) anodized silver, (C) MIP-5-FU/Ura adduct, (D) MIP- 5-FU, (E) MIP-Ura, and (F) side view of MIP-nanoarrays.

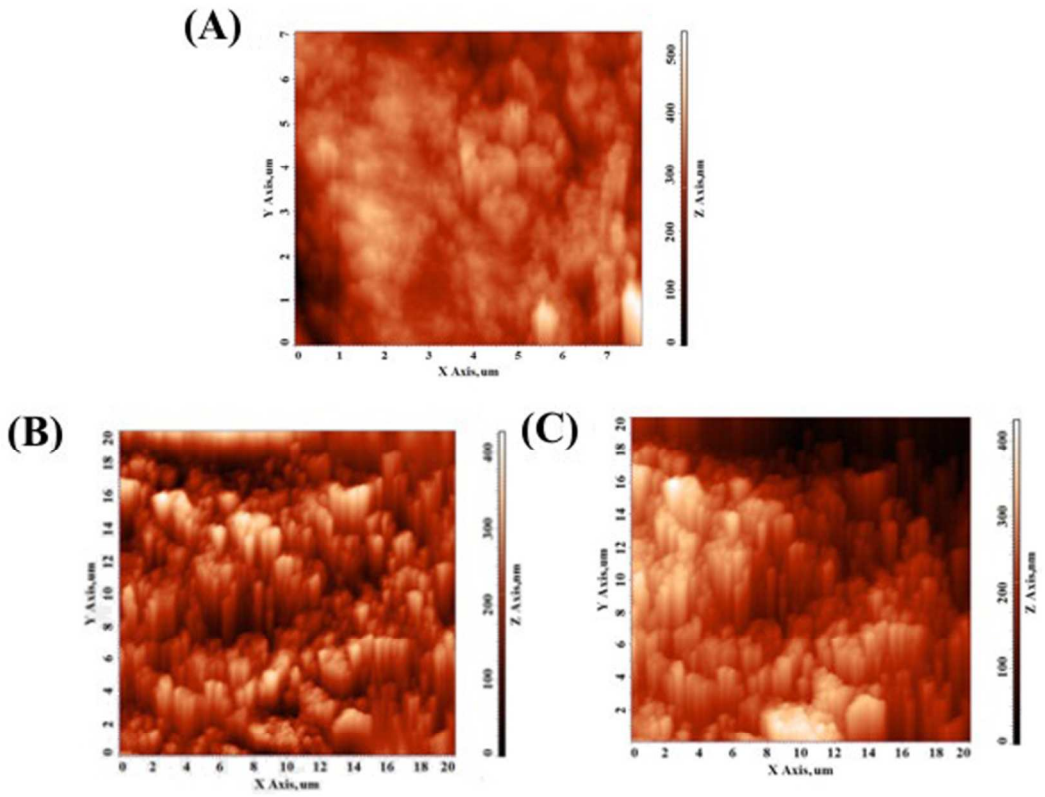

Fig. 4 AFM images: (A) MIP-adduct (Ura/5-FU), (B) MIP-Ura, and (C) MIP-5-FU nanoarrays.

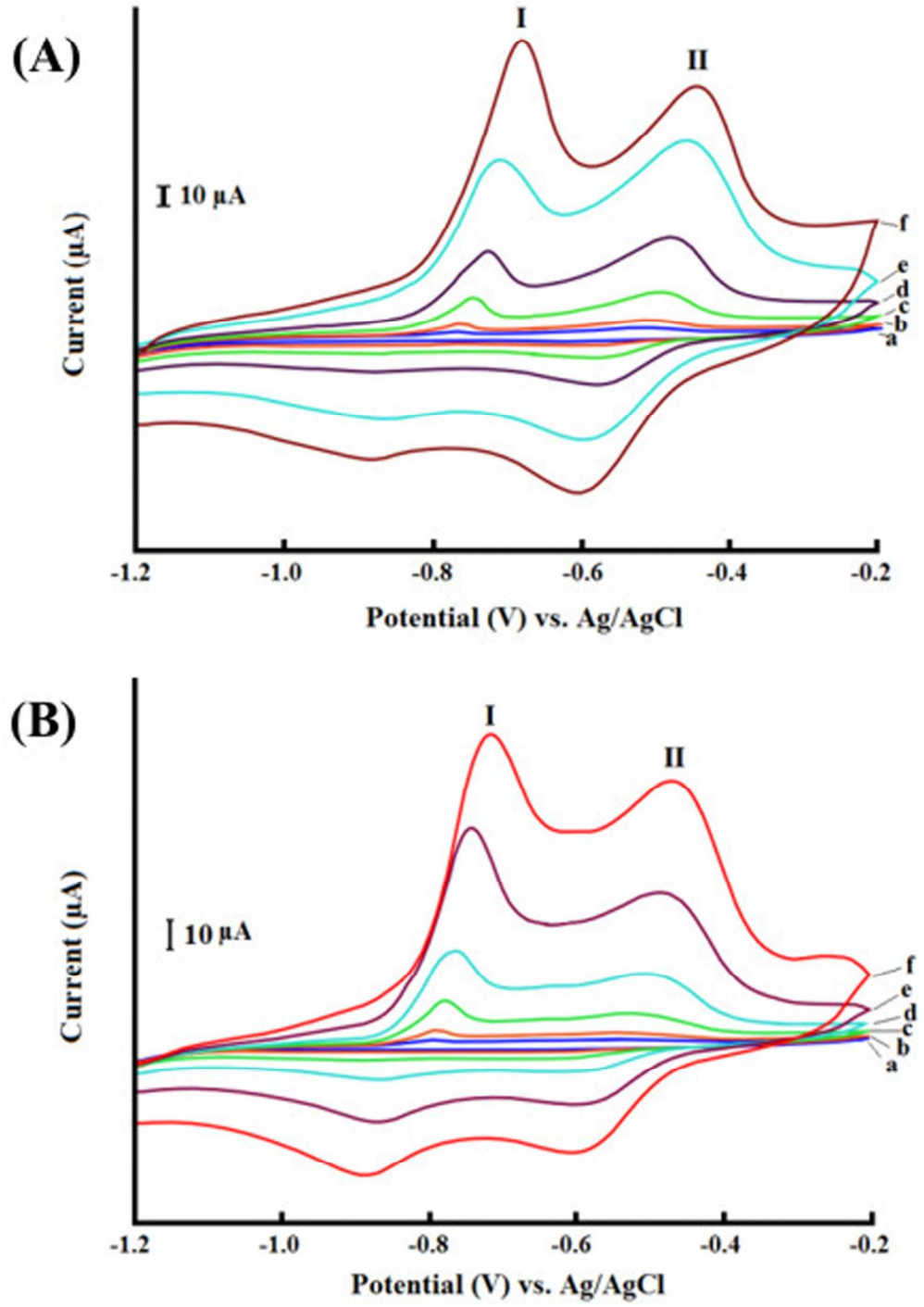

Fig. 5 CV runs of 9.90 ng mL^{-1} Ura (A) and 5-FU (B) at different scan rates: (a) 10, (b) 20, (c) 50, (d) 100, (e) 200, and (f) 500 mVs^{-1} at MIP-nanoarrays electrode (Operating conditions: E_{acc} -1.2V (for Ura/5-FU) *vs*. Ag/AgCl, t_{acc} 210 s, pH 5.6).

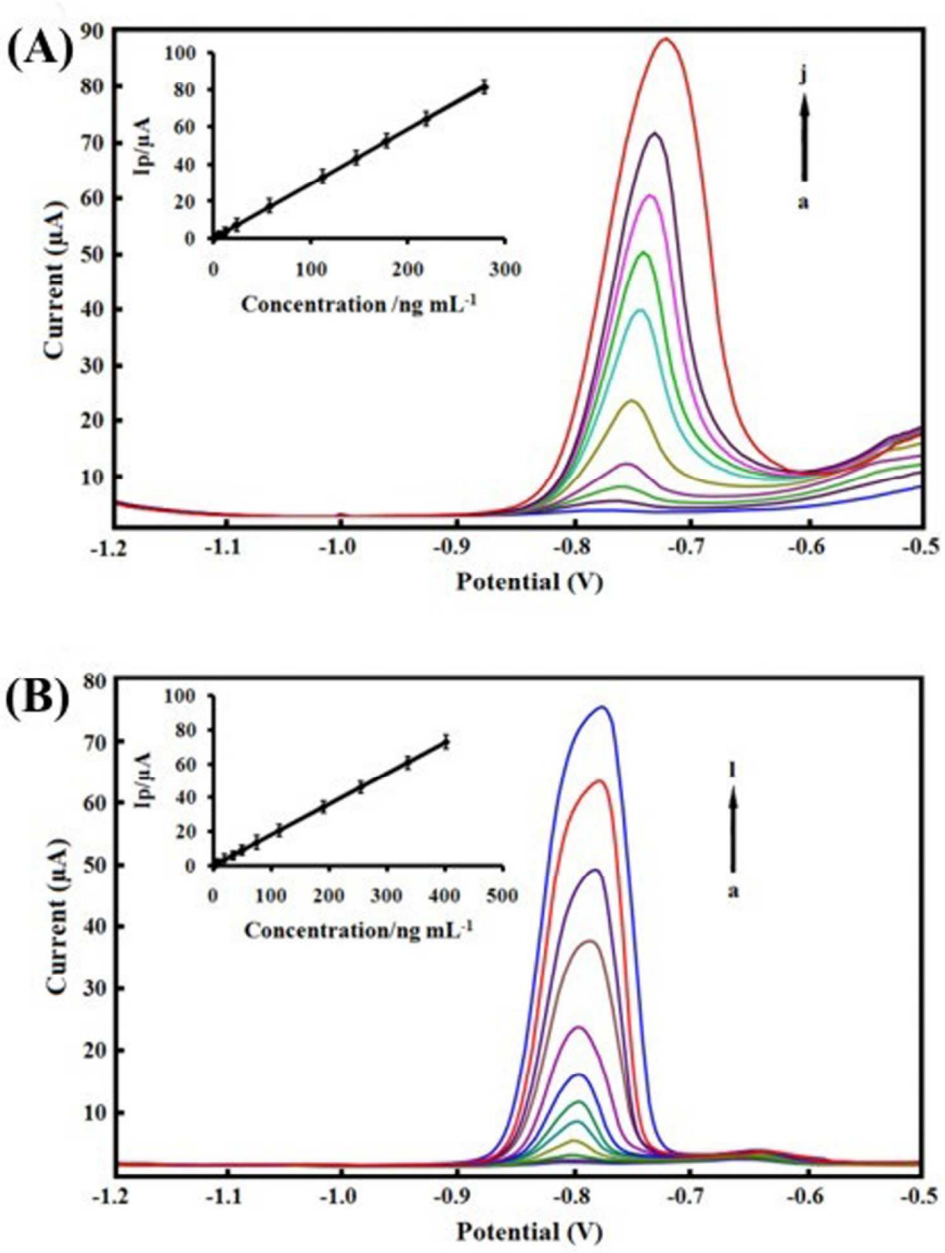

Fig. 6 DPASV responses of Ura (A) and 5-FU (B) at MIP-nanoarrays electrode. Ura concentrations (from a-j): 1.49, 5.44, 12.19, 23.80, 57.80, 112.34, 146.60, 177.70, 218.64, and 278.76 ng mL^{-1}; and 5-FU concentration (from a-l): 1.33, 3.24, 6.41, 17.59, 32.60, 49.11, 73.96, 112.68, 189.26, 253.42, 335.23, 401.15 ng mL^{-1} [Operating conditions: E_{acc} -1.2V, t_{acc} 210s, supporting electrolyte disodium tetraborate solution (pH 5.6), pulse amplitude 25mV, scan rate 10 mVs^{-1})], in aqueous samples.

Table 1 Sample behavior

Analyte/s	Sample	Regression equation	Range (ng mL^{-1})	Recovery[a] (%)	*LOD*[b] (3σ) (ng mL^{-1})	*RSD*[c] (%) (n= 3)
Ura	Aqueous solution	I_P = (0.292±0.001) C + (0.269 ±0.1409), n = 10, R^2 = 0.99	1.49-278.76	97.3-101.1	0.502	0.30
	Blood Plasma	I_P = (0.300±0.0001) C + (0.002 ±0.023), n = 10, R^2 = 0.99	1.428-214.77	97.0-99.6	0.439	0.06
	Pharmaceutical	I_P = (0.301±0.0004) C + (0.082 ± 0.046), n = 10, R^2 = 0.99	1.74-216.67	96.7-100.6	0.617	0.20
5-FU	Aqueous solution	I_P = (0.18 ±0.0001) C + (0.042 ±0.034), n = 12, R^2 = 0.99	1.33-401.15	97.0-101.1	0.331	0.10
	Blood plasma	I_P = (0.180±0.0009) C + (-0.004 ±0.017), n = 7, R^2 = 0.99	2.36-351.11	97.9-100.2	0.663	0.04
	Pharmaceutical	I_P = (0.180±0.0001) C + (0.045 ±0.028), n =7, R^2 = 0.99	1.99-364.69	98.1-100.8	0.482	0.08

[a] % Recovery = (amount of analyte determined / amount of analyte taken) x 100
[b] *LOD* based on the minimum distinguishable signal for lower concentrations of analyte (*S/N*=3, 95% confidence level).
[c] *RSD* (%) for three sets of *LOD* data.

Table 2 The selectivity coefficients (k) and relative selectivity coefficients (k') values obtained on the modified nanoarray sensor.

Compound	**MIP**		**NIP**			
	k_1	k_2	k_1	k_2	k'_1	k'_2
Ura	−	0.00057	0.015	0.025	66.66	0.02
5-FU	0.0034	−	0.007	0.013	0.42	76.92
Ade	0.00017	0.0004	0.001	0.026	0.17	0.01
Gua	0.00034	0.0017	0.003	0.007	0.11	0.24
Cyt	0.00017	0.00028	0.039	0.007	0.02	0.04
Thy	0.00051	0.0014	0.001	0.023	0.02	0.06
DA	0.00034	0.00057	0.013	0.005	0.06	0.11
Hypo	0.00017	0.00028	0.013	0.005	0.03	0.05
BA	0.00051	0.00057	0.008	0.045	0.01	0.01
AA	0.00017	0.0022	0.015	0.014	0.01	0.15
Caff	0.00172	0.00028	0.027	0.057	0.03	0.004
UA	0.00155	0.00086	0.012	0.053	0.02	0.01
Cret	0.00224	0.00028	0.022	0.020	0.11	0.14
Urea	0.00034	0.0086	0.012	0.028	0.02	0.30
Glu	0.00017	0.0057	0.010	0.017	0.02	0.33

k_1= selectivity coefficient was calculated as $i_{\text{interferent}}/i_{\text{Ura}}$ (μA)
k_2 = selectivity coefficient was calculated as $i_{\text{interferent}}/i_{\text{5-FU}}$ (μA)
k'= relative selectivity coefficient was calculated as $k_{1\ \text{MIP}}/\ k_{1\ \text{NIP}}$

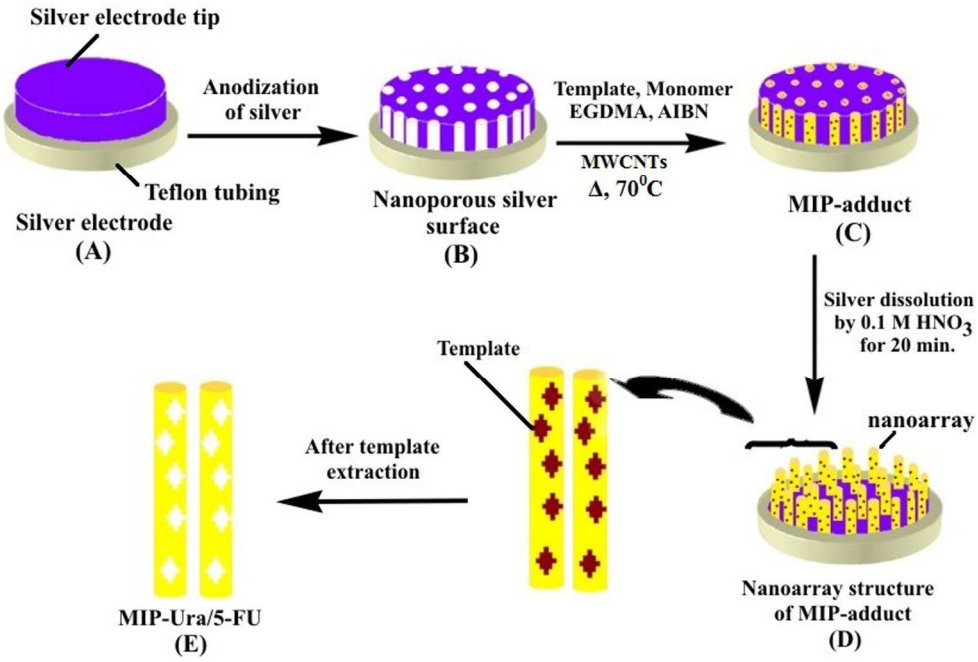

Graphical representation of development of MIP-nanoarrays
98x69mm (600 x 600 DPI)